J Solid State Electrochem (2012) 16:703–714
DOI 10.1007/s10008-011-1421-9

ORIGINAL PAPER

Electrochemical testing of composite electrodes of $(La_{1-x}Sr_x)_sMnO_3$ and doped ceria in NO-containing atmosphere

Rebecka M. L. Werchmeister · Kent Kammer Hansen · Mogens Mogensen

Received: 25 March 2011 / Revised: 25 April 2011 / Accepted: 26 April 2011 / Published online: 7 May 2011

Abstract The possibility of using electrochemical cells for removal of NO_x from an exhaust gas with excess O_2 has been examined. $(La_{1-x}Sr_x)_sMnO_3$ (LSM) and ceria doped with Pr or Gd were selected as electrode materials and investigated in three-electrode cells. The electrodes were characterised electrochemically with electrochemical impedance spectroscopy (EIS) and cyclic voltammetry (CV), and the gas composition monitored while the electrodes were polarised. The electrodes of $(La_{0.5}Sr_{0.5})_{0.99}MnO_3$ (LSM50) and $Ce_{0.8}Pr_{0.2}O_{2-\delta}$ exhibit higher current densities in 0.1% NO in Ar than in air at 300 to 400 °C during CV. This indicates some apparent selectivity towards NO compared to O_2. The electrodes can remove NO, when polarised to at least −0.6 V vs. Pt/Air at 600 °C, and EIS measurements under polarisation indicate that the kinetics of the electrodes change, when the electrode potential gets below −0.6 V vs. Pt/Air.

Keywords Composites · Electrical properties · CeO_2 · Perovskites · Electrochemical deNO_x

Introduction

Nitrogen oxides are formed from N_2 and O_2 present in the atmosphere at the high temperature in combustion engines. Nitrogen oxides take part in the formation of acid rain, they are dangerous to the health of humans and N_2O is a known greenhouse gas. Therefore, great effort is taken in removing nitrogen oxides from exhaust gas. A three-way catalytic converter can remove NO_x in engines running with a low air to fuel ratio, but this is not possible in an engine running lean due to the surplus of O_2 in the exhaust.

Pancharatnam et al. [1] proved that NO could be decomposed by applying a voltage over a Pt|yttria-stabilised zirconia (YSZ)|Pt cell. The F-centers formed on the YSZ surface were suggested as the active sites and this was later confirmed [2].

Since then, many studies in electrochemical removal of nitrogen oxides have been done [3–5], but the great obstacle is still to achieve acceptable current efficiencies (CE) for NO reduction, while O_2 is present.

The wish is to remove NO with a solid oxide electrochemical cell, by reduction of NO to N_2 at the cathode, according to Eq. 1. Then, the oxide ions are transported through the electrolyte and oxidised to O_2 at the anode, Eq. 2. Figure 1 shows a sketch of this type of cell.

$$\text{Cathode}: NO + 2e^- \rightarrow \tfrac{1}{2}N_2 + O^{2-} \quad (1)$$

$$\text{Anode}: O^{2-} \rightarrow \tfrac{1}{2}O_2 + 2e^- \quad (2)$$

Oxygen is present in the exhaust in much higher concentrations than NO_x, and therefore the materials used for catalyst should preferable have high selectivity toward NO_x, in order to avoid wasting power for pumping O_2 through the cell, i.e. the reaction of Eq. 3 should not take place at the cathode.

$$\tfrac{1}{2}O_2 + 2e^- \rightarrow O^{2-} \quad (3)$$

Several perovskites can catalyse the direct decomposition of NO: examples from the literature are $La_{0.8}Sr_{0.2}CoO_3$

R. M. L. Werchmeister · K. K. Hansen (✉) · M. Mogensen
Fuel Cells and Solid State Chemistry Division,
Risø National Laboratory for Sustainable Energy,
Technical University of Denmark,
Roskilde 4000, Denmark
e-mail: kkha@risoe.dtu.dk

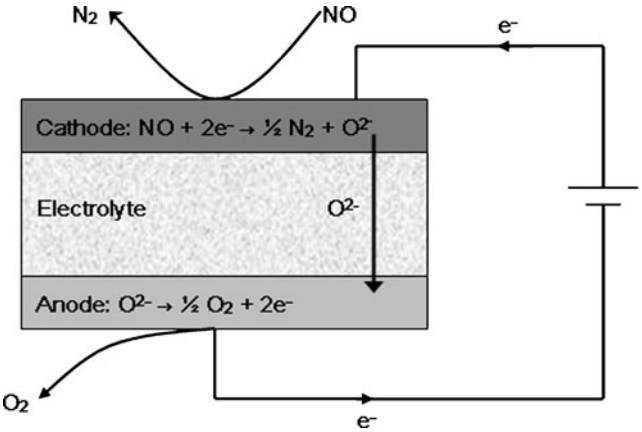

Fig. 1 A sketch of a solid oxide electrochemical cell for removal of NO*x*

and $La_{0.4}Sr_{0.6}Mn_{0.8}Ni_{0.2}O_3$ [6], $La_{0.7}Ba_{0.3}Mn_{0.8}In_{0.2}O_3$ [7], $La_{1-x}Sr_xM_{1-y}M_yO_3$ (M = Co, Ni, Cu) [8], and $La_{0.8}Sr_{0.2}Co_{0.9}Ru_{0.1}O_3$ [5] has also been used as electrode materials for electrochemical removal of NO. $La_{1-x}Sr_xMnO_3$ is used for cathodes for solid oxide fuel cells (SOFCs) and has previously been used as electrode material for electrochemical removal of NO_x [5].

Ceria doped with praseodymium is a material, which has been used for a wide number of applications, such as SOFC electrodes [9], gas sensors [10] and soot oxidation [11]. The Pr ions can easily change oxidation state between +3 and +4; therefore, it is possible that the material has some catalytic activity.

This work is part of an explorative investigation of the $(A_{1-x}A'_x)_{1-\delta}B_{1-y}B'_yO_3$–$M^h_{1-z}M^d_zO_2$ perovskite electrode system with respect to possibilities of finding combinations that might work as NO reduction electrodes. A and A′ are large A-site ions and B and B′ small B-site ions in the ABO_3 type perovskite, M^h and M^d are the metal host ion and dopant ion in the MO_2-type fluorite.

Two sets of relative different materials within the same family were studied, $(La_{0.5}Sr_{0.5})_{0.99}MnO_3$ (LSM50) and $Ce_{1-x}Pr_xO_{2-\delta}$ (CPO) (x=0.1, 0.2) and $(La_{0.85}Sr_{0.15})_{0.9}MnO_3$ (LSM15) and $Ce_{0.9}Gd_{0.1}O_{1.95}$ (CGO10). Both LSM15 and LSM50 are A-site understoichiometric. The LSM50 has a significant higher electronic conductivity (p-type) than LSM15 (σ_{LSM15}=120 S cm^{-1} and σ_{LSM50}=500 S cm^{-1} at 600 °C [12]). CGO10 has a negligible electronic conductivity while CPO has a low but significant p-type electronic conductivity (σ_e for CPO20 is around 1.6×10^{-2} S cm^{-1} at 600 °C [13]).

This testing of different sets of composite electrodes, that have potential for activity towards the electrochemical removal of NO, is a kind of digging down into two different sites in a corner of the vast field of the ABO_3-MO_2-composite electrodes.

Experimental

The composite working electrodes were screen printed onto three-electrode-cell electrolyte, which is sketched in Fig. 2. The materials were either synthesised by glycine nitrate combustion [14] (LSM50, $Ce_{0.9}Pr_{0.1}O_{2-\delta}$ (CPO10) and CPO20) or commercial: LSM15 from Haldor Topsøe A/S and CGO10 from Rhodia. The synthesised metal oxide powders were calcinated at 1,000 °C and 1,200 °C for the CPO and LSM50, respectively. Afterward, the powders were determined to be single phased with X-ray powder diffraction on a Stoe theta-theta diffractometer.

Inks for screen printing were prepared by ball milling the metal oxide powders together with a solvent (terpineol) and a binder. The particle size distribution (PSD) of the inks was measured with a Beckman Coulter Particle Size Analyzer, and the final inks had a PSD with d_{90} smaller than 7 μm.

The three-electrode pellets were pressed from YSZ powder and sintered.

Afterwards, the pellets were cut into the shape displayed in Fig. 2, and the geometry of the pellet and placement of reference electrode is based on the calculation from [15].

To check the reproducibility of the electrodes, symmetrical cells with the same electrodes fabricated in the same manner as described above was also made. The reproducibility of these electrodes was shown to be high. The results have been published elsewhere [16] (Table 1).

The perovskite are all A-site deficient, with 1% and 10% excess Mn. There are one reason for this approach. First of all, this is done in order to prevent the formation of non-

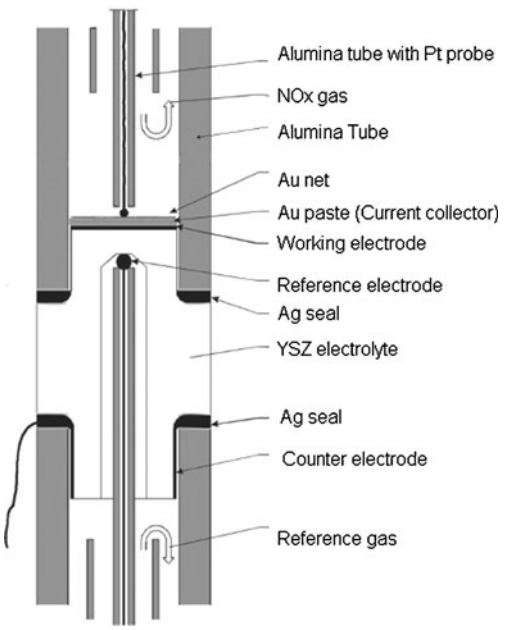

Fig. 2 Sketch of the three-electrode setup

Table 1 The composition of the screen printed electrodes

Electrode	Composition
LSM50/CPO10	50 wt.% $(La_{0.5}Sr_{0.5})_{0.99}MnO_3$+ 50 wt.% $Ce_{0.9}Pr_{0.1}O_{2-\delta}$
LSM50/CPO20	50 wt.% $(La_{0.5}Sr_{0.5})_{0.99}MnO_3$+ 50 wt.% $Ce_{0.8}Pr_{0.2}O_{2-\delta}$
LSM15/CGO10	50 wt.% $(La_{0.85}Sr_{0.15})_{0.9}MnO_3$+ 50 wt.% $Ce_{0.9}Gd_{0.1}O_{1.95}$

conductive phases, such as $SrZrO_3$ and $La_2Zr_2O_7$ at the electrolyte–electrode interface [17].

Three-electrode setup

Gold paste was painted on the working electrode as a current collector, and 20 wt.% carbon was added to the gold paste as a pore former. Furthermore, gold net was placed on the gold paste as a current collector. The counter electrode was Pt paste painted on the YSZ pellet. The working electrode is circular with a diameter of 7.2 mm, corresponding to an electrode area of approximately 0.4 cm^2. The three-electrode cell is placed between the two alumina tubes as shown in Fig. 2, and Ag was used as sealing between the YSZ pellet and the alumina tubing.

The alumina tubes are inside a quartz tube with an inert atmosphere (Ar) which again is placed in a tube furnace.

The atmosphere at the anode and cathode are separated. Air was used as a reference gas at the anode compartment, while gas mixtures of Ar, NO and O_2 was used in the cathode compartment.

The gas flow was 5 mL/min unless otherwise stated. The gas mixtures used was: 0.1% NO in Ar, 0.1% NO+5% O_2 in Ar and 20% O_2 in Ar. Around 0.1% to 0.2% O_2 was also present, detected by mass spectrometer, due to leaks in the gas inlet. The gas flows were controlled by mass flow controllers from Brooks.

The setup was placed inside a vertically mounted furnace, and the measurements were done in the temperature range of 300–600 °C. A quadrupole mass spectrometer, OmniStar from Pfeiffer, was used to monitor the gas composition in the outlet gas.

The electrochemical measurements were done with a Gamry Femtostate.

Measurements were also performed using symmetrical cells as described elsewhere [17].

Electrochemical techniques

The electrodes were subjected to EIS. The lowest frequency used was 1 mHz, and the highest 100 kHz. The impedance spectroscopy was applied both at electrodes at open circuit voltage (OCV) and under cathodic potential. An amplitude of 36 mV root mean square was used.

Further, cyclic voltammetry was applied to the electrodes. A sweep rate of 5 mV/s was used, and the limits were −0.8 V and 0.8 V, and in some cases −1 V and 1 V relative to the reference electrode (Pt/air). The voltammograms were only IR corrected when stated. The electrodes were also polarised for 1 or 2 h under −0.8 to −1 V relative to the reference electrode (Pt/air).

The impedance data were analysed with the software "Equivalent circuit for Windows" from University of Twente [18].

Results

OCV

The OCV varied as a function of the gas flow, see Fig. 3. The lowest value for OCV obtained in an atmosphere containing 0.1% NO in Ar was around −0.155 V vs. Pt/air, so the electrodes are not changing composition very much due to low pO_2.

The theoretical OCV was calculated with the Nernst equation from the amount of O_2 present at the cathode measured by mass spectrometry, assuming only Eq. 2 takes place.

EIS and equivalent circuits

The impedance spectra recorded at OCV were fitted to equivalent circuits having between two and four arcs depending on temperature and atmosphere; see Figs. 4 and 5 for examples. All the arcs were best described by an ohmic resistance in parallel with a constant phase element (CPE) as defined in Eq. 4 [19].

$$Z = 1/(Y_0(j\omega)^{\alpha} \tag{4}$$

Where Y_0 and α are constants. An equivalent capacitance (EC, C_ω) can be calculated for the CPE, see Eq. 5 [20].

$$C_\omega = R^{(1-\alpha)/\alpha}Q^{1/\alpha} \tag{5}$$

The impedance spectra for the working electrodes of the three-electrode pellets were fitted with the equivalent circuits found in earlier studies with symmetrical cells for the same type of electrode and experimental conditions [17].

The impedance spectra typically consist of one to two small high-frequency arcs and a larger middle-frequency (MF) arc. When the atmosphere is NO in Ar, a low-frequency (LF) arc is also found.

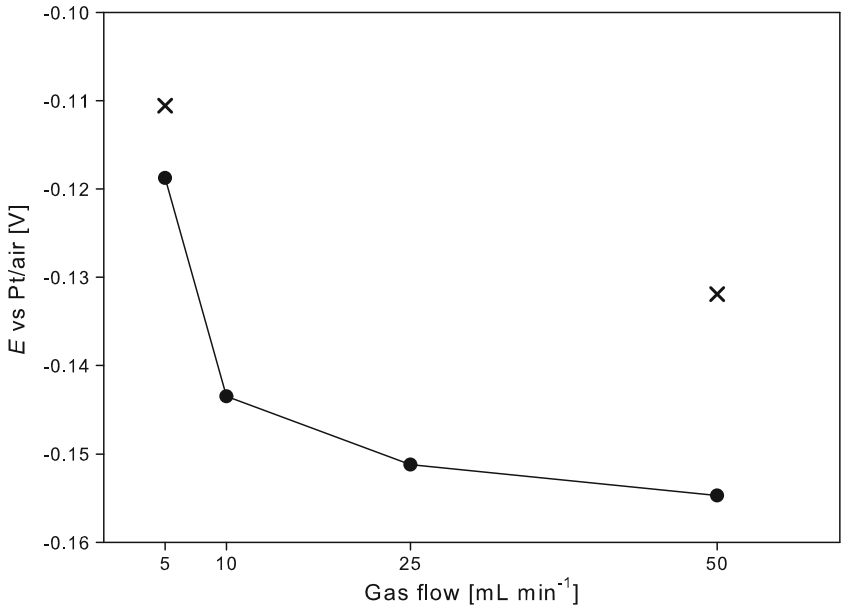

Fig. 3 OCV as a function of flow rate for the LSM50/CPO10 electrode in 0.1% NO in Ar at 600 °C. Calculated OCV (*x*) from pO_2 using the Nernst equation with Eq. 2. The calculated OCV varies with flow rate due to the presents of leaks

Figure 4 shows the impedance spectra for the symmetrical cells in 1% NO in Ar at 600 °C. The ohmic resistance, R_s, found in the impedance spectra for the cells was very large, around 70 Ω at 600 °C due to the part of the YSZ electrolyte between the reference electrode and the working electrode; see Fig. 2. Ohmic resistance is resistance that is not associated with the working electrode reaction.

During polarisation of the cell, the electrode potential, $E_{\text{electrode}}$ can be found from Eq. 6 and in Fig. 6 an example of the changes in a cyclic voltammogram due to correction of R_sI losses is shown. When the imposed potential is −1 V vs. air/Pt, the actual electrode potential is only −0.8 V vs. Pt/Air.

$$E_{\text{electrode}} = E - R_sI \tag{6}$$

The determination of R_s at 300 °C is difficult because at such low temperatures, HF arcs can be found in the impedance spectra, which might result from the electrolyte, and therefore these resistances are a part of R_s. The arc with an EC around 2×10^{-10} F cm^{-2} results from grain boundaries in the electrolyte or capacitance in the equipment and the other arc with an EC around 3×10^{-8} F cm^{-2} results from the transfer of oxide ions into the electrolyte. The first arc is part of the R_s, while the second is not. Therefore, the R_s is around 12 kΩ cm^2 at 300 °C as seen in Fig. 5b.

Cyclic voltammetry

The current density is higher in the anodic region than in the cathodic region for all the electrodes regardless of temperature and atmosphere. Further, the current density decreases with decreasing temperature.

All the electrodes had higher cathodic current densities in air than in 0.1% NO in Ar or 0.1% NO + 5% O_2 in Ar at 600 °C; see Fig. 7a. However, this changed when the temperature decreased. The current density for electrodes in NO+O_2 was higher than for electrodes in air in the temperature range of 300–500 °C for all the electrodes,

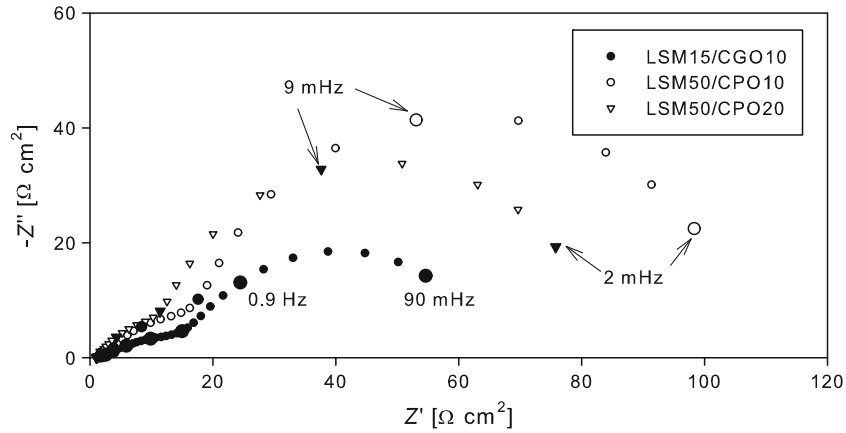

Fig. 4 Impedance plot for symmetrical cells with LSM15/CGO10, LSM50/CPO10 and LSM50/CPO20 electrodes in 1% NO in Ar, 100 mL/min flow at 600 °C

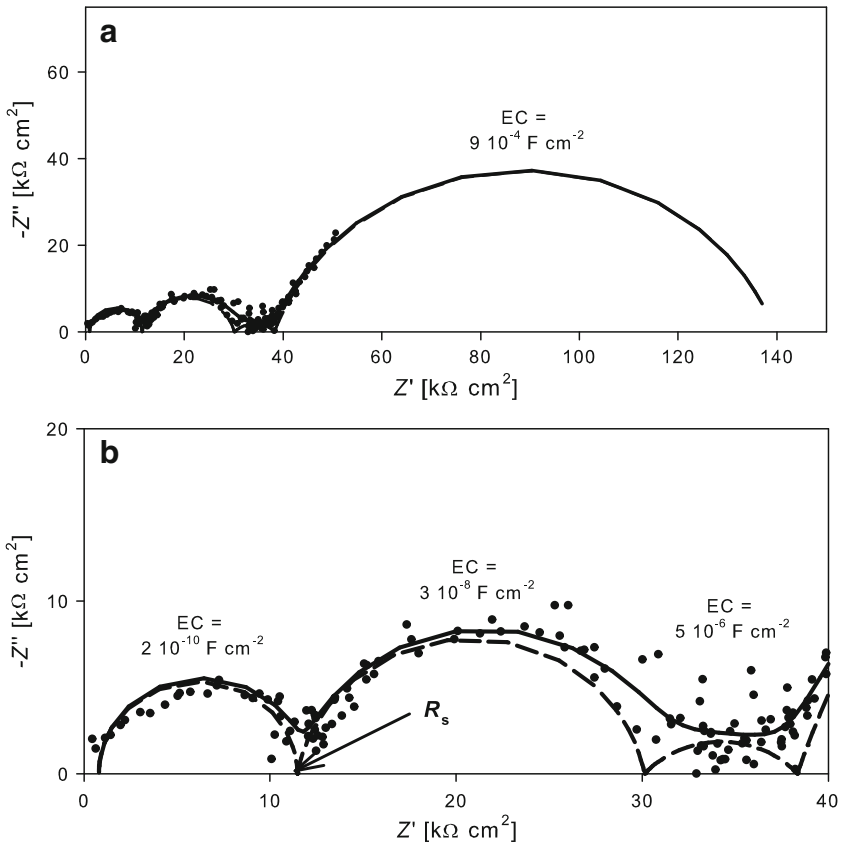

Fig. 5 **a** Impedance spectra for LSM15/CGO10 electrodes in air at 300 °C along with the deconvolution of the data. **b** Magnification of the high-frequency arcs marked with their EC. The summit frequency of the two high-frequency arcs are: 70 kHz and 300 Hz.

while the current density for electrodes in NO in most cases was higher than air but lower than NO+O_2; see Fig. 7b as an example.

Figure 8 shows cathodic current densities recorded at −0.6 V vs. Pt/air for the electrodes in the temperature range of 300–600 °C.

Peaks were observed in the voltammograms recorded at 600 °C and in 0.1% NO for all the electrodes; see Fig. 6 for an example. When the atmosphere is 0.1% NO and 5% O_2 in Ar or air at 600 °C, then no peaks were found. The same is seen for cyclic voltammograms recorded at lower temperature.

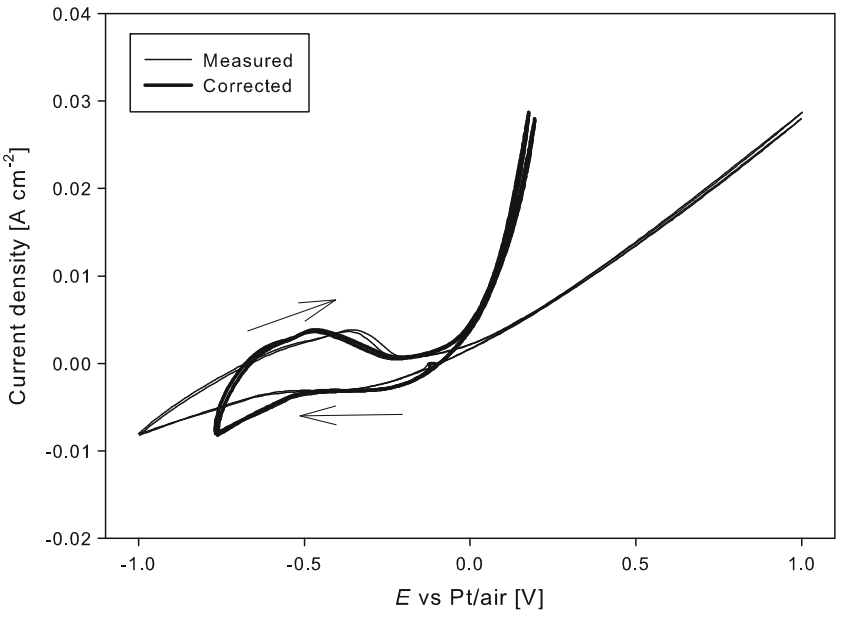

Fig. 6 Cyclic voltammogram for LSM50/CPO10 electrodes cells in 0.1% NO in Ar at 600 °C. The thin line represents the measured data and the thick line the data with the R_sI losses have been subtracted from the potential

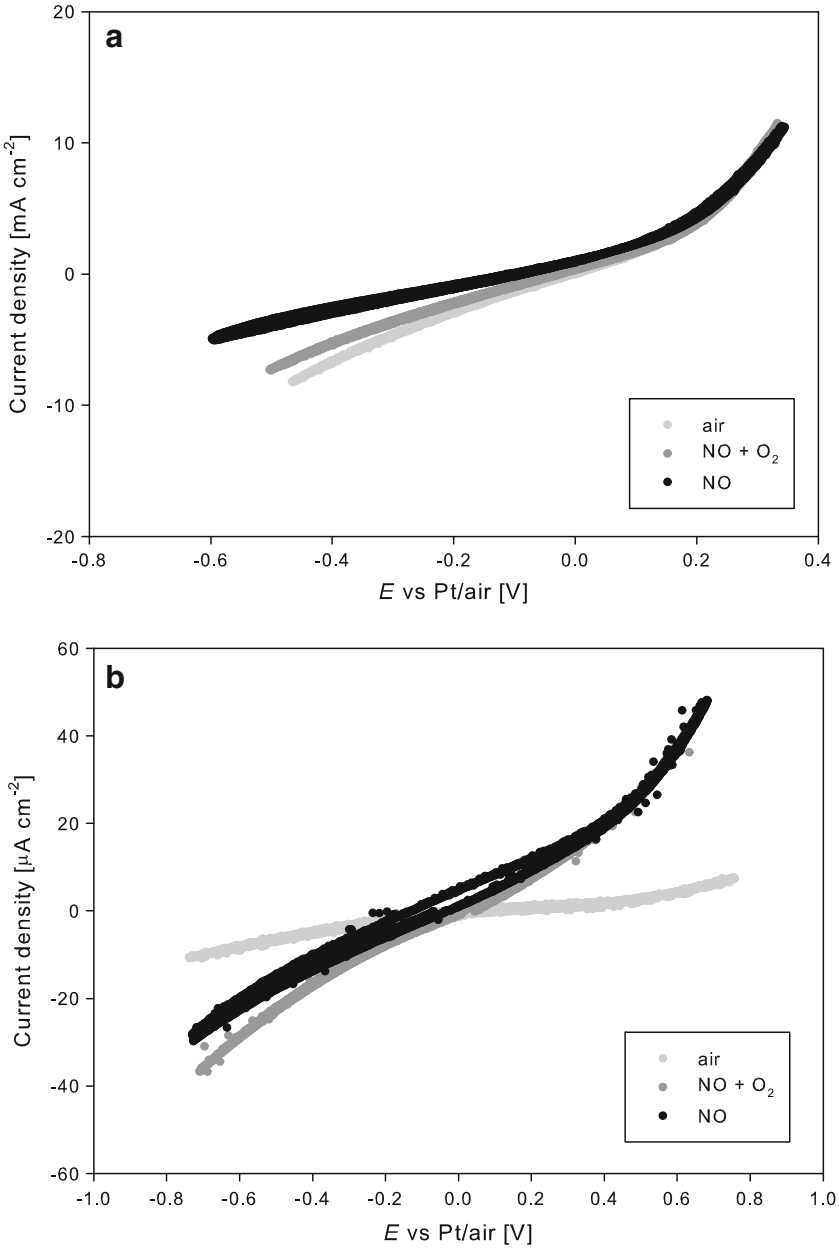

Fig. 7 Cyclic voltammogram for LSM50/CPO20 electrodes in air (grey), 0.1% NO + 5% O_2 in Ar (*dark grey*) and 0.1% NO in Ar (*black*) at 600 °C (**a**) and 500 °C (**b**)

Polarisation of electrodes

When the electrodes were polarised, it was possible to observe conversion of NO with the mass spectrometer at 600 °C for 0.1% NO in Ar for all three types of electrodes. During polarisation, a decrease in the O_2 concentration was also seen. The conversion degree along with the CE for each type of electrodes can be seen in Table 2.

The CE is defined as the ratio between the amount of NO molecules removed as measured by mass spectrometer to the theoretical amount of NO reduced, $I/(2F)$, where F is Faradays constant, calculated from the current consumption, assuming two electrons per reduced NO molecules as seen in Eq. 1.

The three types of electrodes were also polarised to −0.8 V vs. air/Pt (IR corrected) at 600 °C in 1,000 ppm NO +5% O_2 in Ar, and no gas conversion was detected with the mass spectrometer.

For the cell with LSM15/CGO10 and LSM50/CPO10 electrodes in 0.1% NO in Ar, the polarisation was varied, and a decrease in NO concentration was detected from around −0.6 V vs. Pt/Air over the electrode.

NO conversion and CE can be seen as a function of the polarisation over the LSM15/CGO10 electrode in Fig. 9.

The decrease in the O_2 concentration at polarisation with potentials in the range −0.6 to −0.8 V vs. Pt/air is around 40% independent of polarisation. The LSM50/CPO20 electrode can achieve 12% NO removal at −0.6 V vs. Pt/

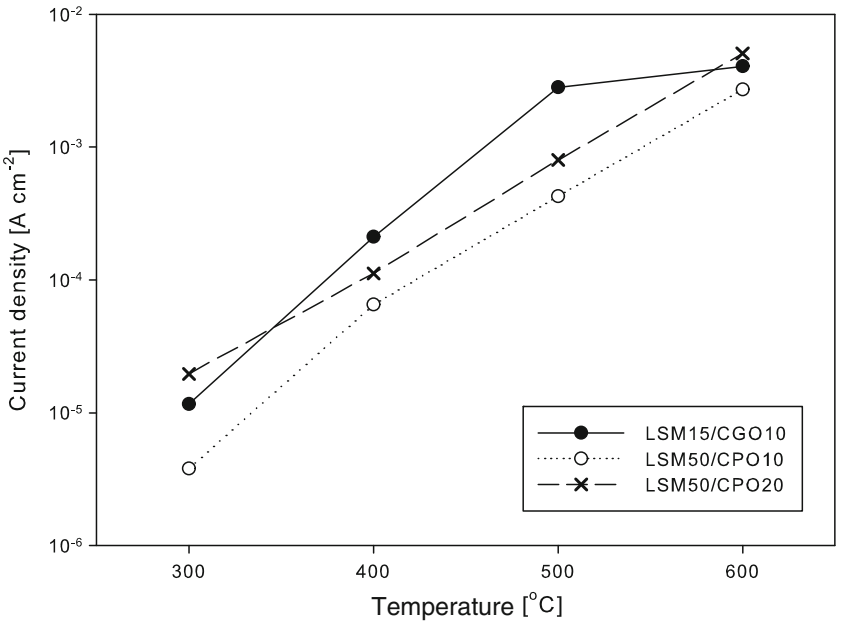

Fig. 8 i_{NO} as a function of temperature for electrodes of LSM15/CGO10, LSM50/CPO10 and LSM50/CPO20 in 0.1% NO in Ar at −0.6 V vs. Pt/air

Air, again with the amount of O_2 reduced being independent of polarisation. The CE also decreases from 35% to 8% in this case.

It was not possible to detect gas conversion at temperatures lower than 600 °C.

EIS under polarisation

An LSM50/CPO20 electrode was subjected to EIS at 600 °C in 0.1% NO in Ar under polarisation at gas flow equal to 5, 10, and 20 mL/min. The polarisation resistance (R_p) increased dramatically when the electrode was polarised; see Fig. 10.

R_p also increases with increasing flow rate, which was also seen for the symmetrical cells. Most of this increase was found in the resistance of the LF arc, R_{LF}, which is believed to be a type of conversion arc caused by low concentration of an intermediate gaseous reactant [17], while the resistance of the MF arc, R_{MF}, which is related to charge transfer, when NO or O_2 is reduced, increases much less.

The EC for the LF arc also varies with the polarisation, as seen in Fig. 11.

Table 2 Degree of NO conversion and CE for polarisation with −0.8 V vs. Pt/Air for electrodes in 1000 ppm NO in Ar, 5 mL/min flow and at 600 °C

Electrode	LSM15/CGO10	LSM50/CPO10	LSM50/CPO20
NO conversion	66%	53%	56%
O_2 present	2,100 ppm	1,700 ppm	1,800 ppm
O_2 removed	41%	28%	22%
N_2 formed	360 ppm	50 ppm	250 ppm
CE	18%	20%	35%
Current density	5.5 mA cm^{-2}	3.4 mA cm^{-2}	2.0 mA cm^{-2}

Discussion

Reaction mechanism

The LF arc in the impedance spectra is seen for electrodes in 0.1% NO in Ar, and it is dependent on gas flow and concentration of NO. This arc is likely a type of conversion arc because of the low frequency, a high α value and the dependence of flow rate [21]. It was found that this arc increases with increasing flow rate in an earlier study [17], the opposite of what would be expected for a conversion arc. Consequently, the LF arc was linked to the low concentration of an intermediate, possible NO_2, which was formed catalytically by the electrode materials. By increasing the flow rate, this intermediate would be flushed away, decreasing its concentration and thereby increasing the R_{LF}.

The change in OCV, when the flow rate is changed shows that electrode reactions, which are affected by flow rate, are taking place. A higher flow rate can dilute intermediates. The atmosphere at the reference electrode is air, so the difference in oxygen partial pressure explains some of the negative OCV. Oxygen could be formed at the cathode according to Eq. 2, and the O_2 concentration decreases with increasing flow rate, as leaks have less influence, which could explain the more negative OCV with higher flow rate as seen in Fig. 3. Likewise, it would

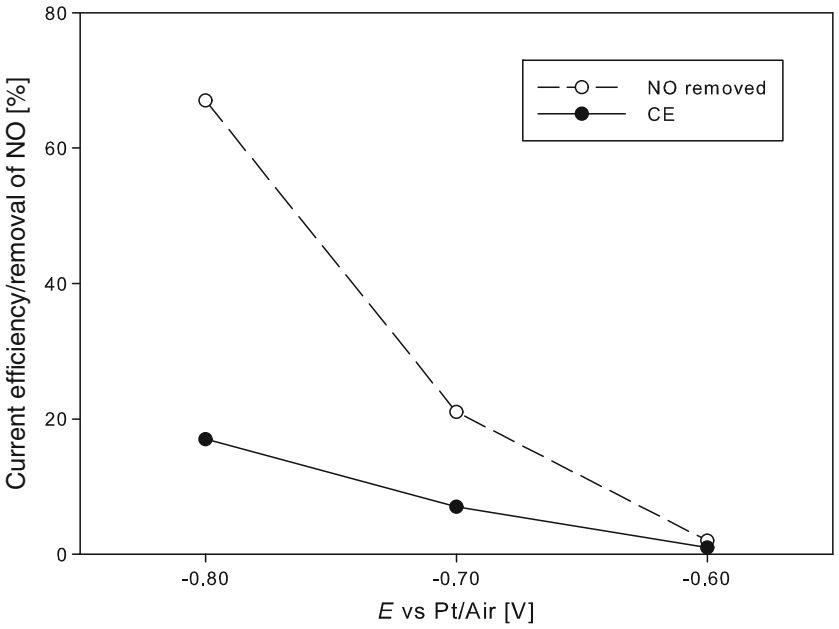

Fig. 9 NO conversion and current efficiency as a function of polarisation for LSM15/CGO10 electrodes in 0.1% NO in Ar at 600 °C

also be possible for NO to react with the oxide ions, as in Eq. 7. This fits well with the hypothesis that low concentration of NO_2, formed by LSM is causing the LF arc, which is flow dependent.

$$NO + O^{2-} \rightarrow NO_2 + 2e^- \quad (7)$$

The measured value for OCV is at a more negative potential than the one calculated from pO_2. The difference between the OCV calculated from pO_2 and the experimental data are small at 5 mL/min, while the difference is larger at a flow of 50 mL/min. If the difference is assumed to be caused by the reaction in Eq. 7, then the NO_2 concentration must be lower at the electrode at a flow of 50 mL/min compared to 5 mL/min as the NO concentration stays the same.

NO_2 can be produced from NO by LSM [22]. This could be through reaction 7, which the OCV measurements seems to indicate or through an equilibrium between NO, NO_2 and N_2O, as shown in Eq. 8. No N_2O was detected with the mass spectrometer, this points to Eq. 7, although it could be that N_2O is below the detectable limit (around 25 ppm).

$$3NO \rightleftarrows N_2O + NO_2 \quad (8)$$

The LF arc completely dominates the impedance spectra for the symmetrical cells in NO. This indicates that NO does not react with the electrode directly electrochemically

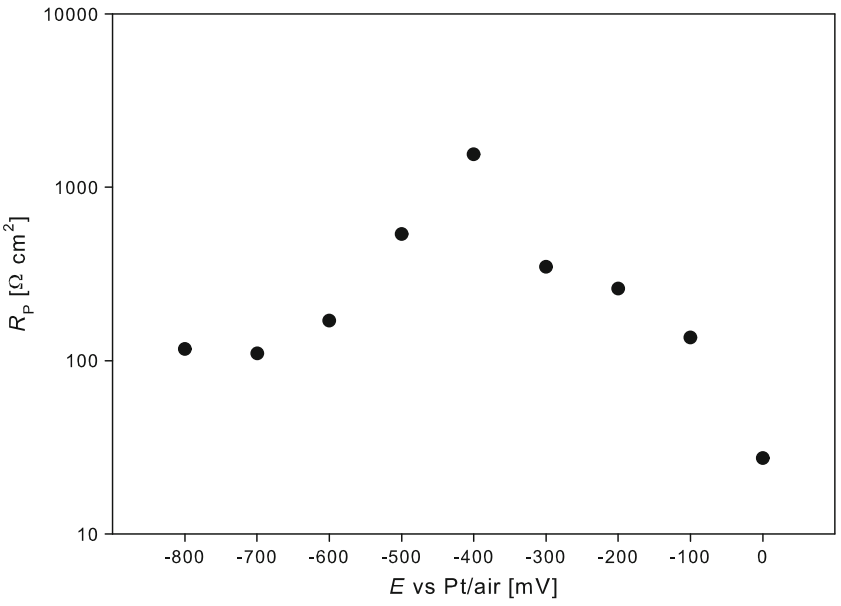

Fig. 10 R_p for LSM50/CPO20 electrode in 5 mL/min 0.1% NO in Ar at 600 °C as a function of potential of the electrode

around OCV at high temperatures. Instead, the electrodes react with an intermediate, possible NO_2, formed catalytically by the electrodes. It is possible to have an equivalent circuit as the one sketched in Fig. 13, where a parallel RQ element exist corresponding to a direct reaction with NO.

But if the R value of the direct reaction is much larger than the one for the reaction with the intermediate, then it will not be visible in the impedance spectra, as it mainly reflects the path of the equivalent circuit with the lowest overall resistance. Figure 4 shows the impedance measurements on symmetrical cells in NO in Ar at 600 °C; from this, the activity for the electrodes is expected to be the following: LSM15/CGO10>LSM50/CPO20>LSM50/CPO10 because the LSM15/CGO10 electrodes have the lowest R_p and LSM50/CPO10 the highest R_p. This is in accordance with the conversions seen in Table 2. So the resistance found from the impedance spectra of the symmetrical cells at OCV can predict the conversion at least at 600 °C. The LF arc dominates the impedance spectra recorded in the NO-containing atmosphere, and therefore makes up most of the R_p. As this arc is connected with low concentration of an intermediate, possible NO_2, this could indicate that the same route of NO removal takes place when the electrodes are polarised.

For the impedance measurements under polarisation, there is a sudden increase in EC, which coincides with the peak of the R_p value; see Figs. 11 and 12. The gas conversion of NO can be detected by mass spectrometry when the electrode is polarised with −0.6 V vs. Pt/air or more; this is the polarisation range where EC is stable with a value around 0.6 F. The same tendency is seen at higher flow rates; however, the peak in R_p and increase in EC is seen at the more negative potential, see Fig. 12.

The electrode does not remove NO in any detectable amounts in the polarisation range of 0 to −0.6 V vs. Pt/air, but some reduction of O_2 does take place. The increasing value of R_{LF} in this region could be due to the low concentration of O_2 as there is only a very small amount present. But the size of R_{LF} does also depend on electrode material, as seen in Fig. 4, which indicate that the materials catalytic properties has an effect as well. This would not be the case if the arc was caused by low concentration of O_2. A parallel reaction with NO through an intermediate could also explain the increasing R_p, especially if this intermediate was a compound like NO_2, which requires an oxidation of NO, as the potential of the electrode becomes more and more reducing.

The increase in EC at −0.6 V vs. Pt/air over the electrode, suggests that at these negative potentials there is a different LF arc present. The reduction of NO starts at this potential and likely proceeds through another, less hindered path, this could be the direct reaction with NO with stippled lines in the equivalent diagram in Fig. 13. The reason for this could be that the electrode composition starts changing at these low potentials.

The increase in N_2 corresponds with what should be expected from (1) for the LSM50/CPO20 and LSM15/CGO10 electrodes see Table 2. This is not the case for the LSM50/CPO10 electrodes, where too little N_2 is formed. The lack of formation of N_2 must mean that some other nitrogen-containing species is formed, which could be nitrates on the surface of the electrode or NO_2 in the gas phase. N_2O formation would be detectable in the mass spectrometer and was not observed during the polarisation, while formation of NO_2 is not detectable with the mass spectrometer.

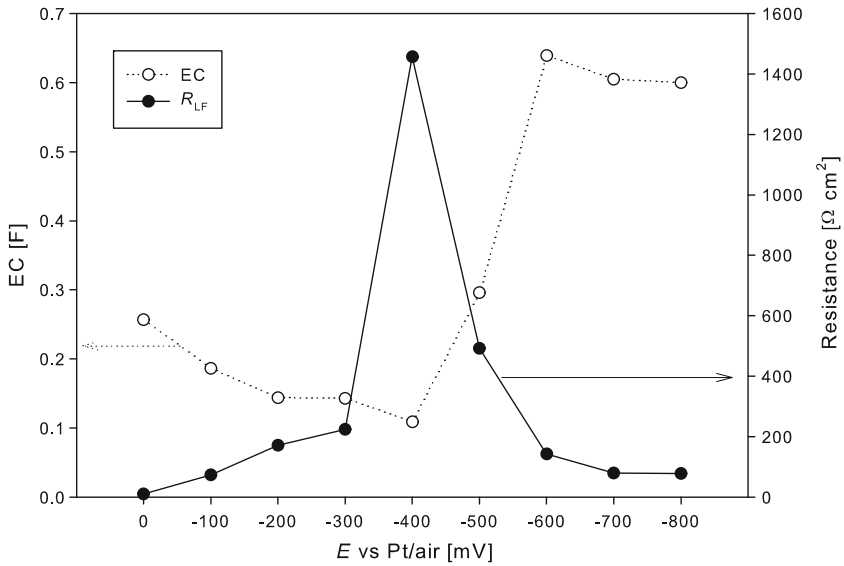

Fig. 11 R_{LF} and EC_{LF} for LSM50/CPO20 electrode in 5 mL/min 0.1% NO in Ar at 600 °C as a function of potential of the electrode

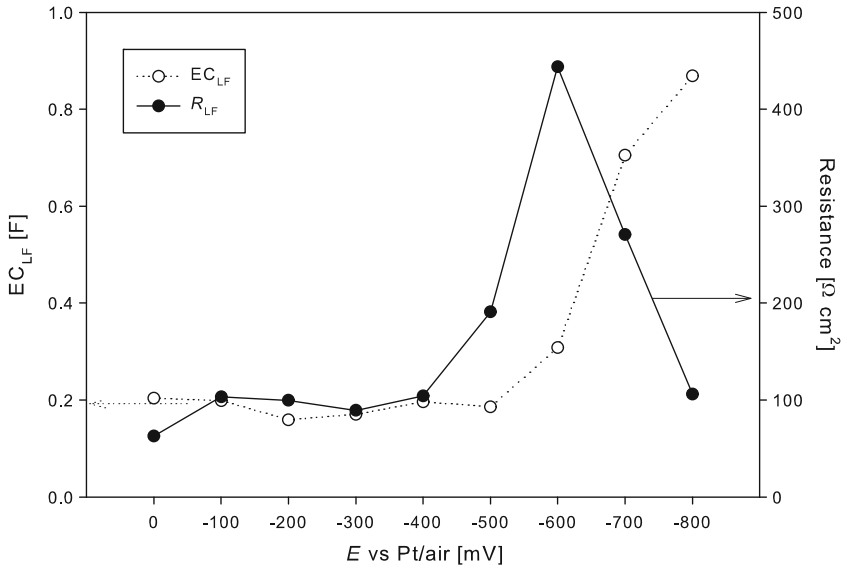

Fig. 12 R_{LF} and EC_{LF} (equivalent capacity) for LSM50/CPO20 electrode in 10 mL/min 0.1% NO in Ar at 600 °C as a function of potential of the electrode

Selectivity

The relationship between the cathodic current densities at a similar potential in different atmospheres obtained from the cyclic voltammograms are used as a measure for selectivity.

When i_{NO} is larger than i_{air} at a similar potential then the electrodes are more active towards NO_x than towards O_2.

Generally, the i_{NO}/i_{air} ratio of the electrodes increases with decreasing temperature, indicating that the electrodes become more selective towards NO with decreasing temperature. Further, the LSM50/CPO20 electrode is more dependent on temperature than the LSM50/CPO10 and LSM15/CGO10 electrodes as seen in Fig. 14.

The ratio between i_{NO} and i_{air} is below or around 1 in the temperature range of 500–600 °C for all electrodes. A higher i_{NO} than i_{air} is seen at 300 °C, for all the electrodes and also at 400 °C for the electrodes with CPO. When O_2 and NO are simultaneously present in the atmosphere, then

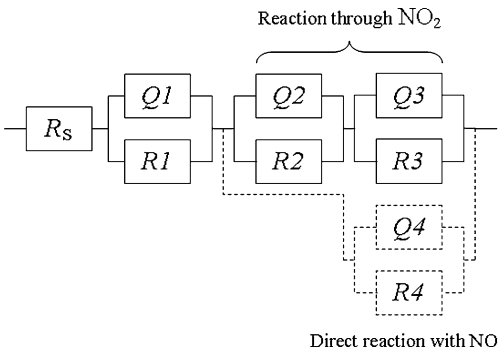

Fig. 13 Potential equivalent circuit diagram for impedance of cells with electrodes of LSM/CPO at 600 °C in 1% NO in Ar. The parallel RQ unit drawn with dotted lines represents a direct reaction between the electrodes and NO, which have higher resistance than (R2Q2) (R3Q3), which represents the reaction with an intermediate such as NO_2

the two species will compete for reaction with the electrode. Preferably, the electrodes should be selective towards NO, and if i_{NO+O2} is larger than i_{air}, then we assume that the electrodes activity towards NO is not hindered by O_2. As there is only 5% O_2 present compared to the 20% in air, then it is not expected that i_{NO+O2} is larger than i_{air} unless the electrodes react with NO or an intermediate originating from NO. The ratio between i_{NO+O2} and i_{air} can be seen in Fig. 15. The LSM50/CPO20 electrode has the highest apparent selectivity at 300 °C, and as the ratio between i_{NO+O2} and i_{air} is well above 1, the apparent selectivity is not hindered by the presence of O_2. The electrodes containing CPO have similar selectivity in the temperature range of 400–600 °C, while the LSM15/CGO10 electrodes generally have lower selectivity except at 600 °C.

Electrodes containing CPO seems to have higher apparent selectivity. This could be due to Pr ions changing oxidation state and thereby being more catalytically active. The general trend with higher selectivity with lower temperature could be caused by change in the reaction mechanism at lower temperature. For the symmetrical cells, the LF arc becomes less dominating with lower temperature, and cannot be found at 300 °C, this indicate that the direct reaction with NO takes place at low temperature.

The discussion about selectivity is based on the assumption that when the ratio between i_{NO+O2} and i_{air} is high, then the electrodes react preferably with NO compared to O_2. There could, however, also be the alternative explanations; that the presence of NO makes the electrode more effective of reducing O_2. Reinhardt et al. [3] suggested that a more reactive oxygen surface species was formed from reaction between O_2 and NO, but the investigations were based on measurements on currents and not gas analysis, therefore the reactive species could just as well have been NO_2 formed from O_2 and NO.

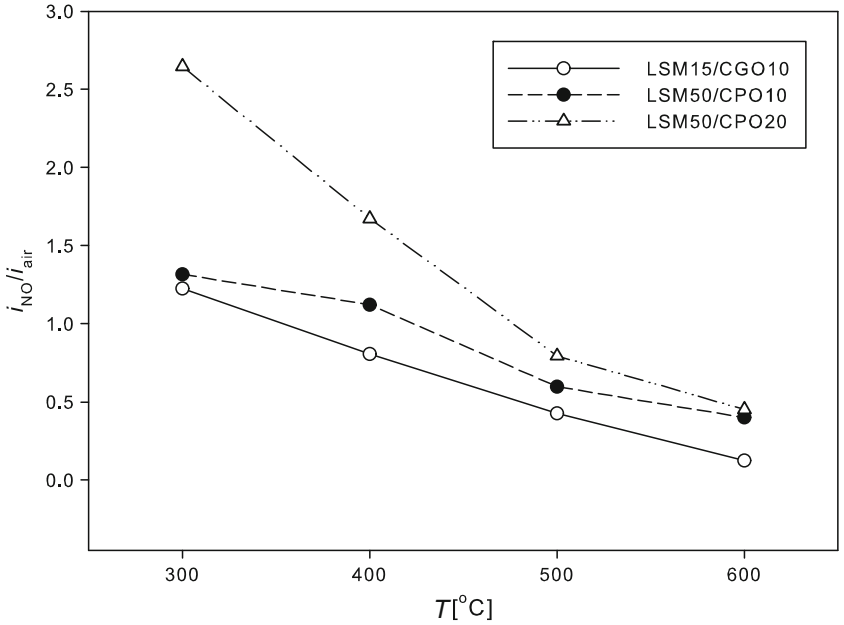

Fig. 14 The ratio between i_{NO} and i_{Air} as a function of temperature for electrodes of LSM15/CGO10, LSM50/CPO10 and LSM50/CPO20

The measurements of i_{NO} in Fig. 8 shows a slightly higher current density for LSM50/CPO20 than for LSM15/CGO10 electrodes, but the LSM15/CGO10 electrodes removed more NO than the LSM50/CPO20 electrodes. The cyclic voltammograms at 600 °C in 0.1% NO are, however, different from the others recorded at lower temperature, due to the cathodic peak. This cathodic peak is likely related to the reduction of NO or formation of nitrates.

The LSM50/CPO20 electrode has the highest CE, almost twice as high as for LSM15/CGO10 electrode. The concentration of O_2 decreases as well during polarisation, due to reduction of O_2, but while the LSM15/CGO10 electrode has a 41% drop in O_2 concentration, then the LSM50/CPO20 electrode only experiences a drop of 22%. This explains the differences in CE.

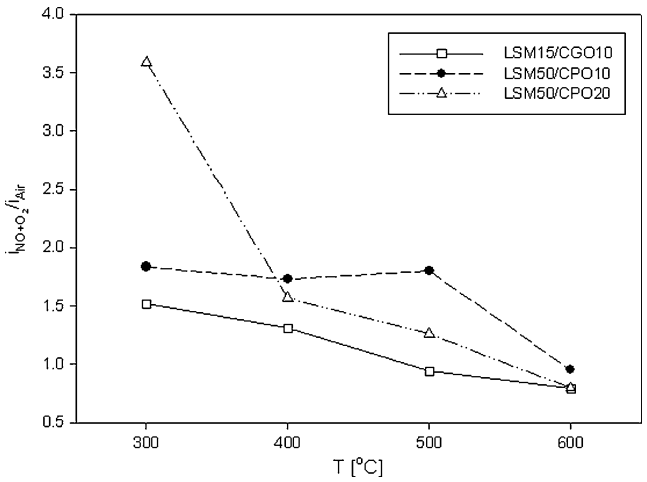

Fig. 15 The ratio between i_{NO+O2} and i_{Air} as a function of temperature for electrodes of LSM15/CGO10, LSM50/CPO10 and LSM50/CPO20

The LSM50/CPO20 electrode shows a high selectivity towards NO compared to O_2, but only at low O_2 concentrations, not when 5% O_2 is present. The order of the electrodes with respect to CE corresponds to the order predicted by Fig. 14, the LSM50/CPO20 electrode which has the highest ratio between i_{NO} and i_{air} also has the highest CE.

If the current achieved at −0.8 V vs. Pt/Air from the cyclic voltammogram for the LSM15/CGO10 recorded at 500 °C electrode is converted into ppm NO removed, assuming the same CE as at 600 °C, then only 12 ppm NO is removed, approximately 1%. The CE is, however, not necessarily the same at lower temperatures. The selectivity seems to be better at 300 °C; so, likely, the CE would also be higher at this temperature, while the selectivity does not change remarkably from 600–500 °C.

Conclusion

The electrodes are not electrochemically active towards NO around open circuit voltage. A conversion arc in the impedance spectra in 0.1% NO is connected with low concentration of an intermediate—possibly NO_2—which react with the electrode instead. The NO_2 can be formed catalytically by the LSM in the electrode, either with small amounts of O_2 present in the atmosphere or from oxide ions from the electrode. The latter is supported by increasingly negative OCV with increasing flow rate, which cannot all be explained by the concentration of O_2. Impedance measurements under polarisation show that the mechanism

changes at more negative potentials, from −0.6 V vs. Pt/Air. It is likely that the electrodes react directly with NO at these low potentials.

All the electrodes tested could remove NO at 600 °C and below −0.6 V vs. Pt/air in an atmosphere of 0.1% NO in Ar, and N_2 was produced. The $(La_{0.85}Sr_{0.15})_{0.9}MnO_3$/$Ce_{0.9}Gd_{0.1}O_{1.95}$ electrode was the most active removing two-thirds of all NO present when polarised with −0.8 V vs. Pt/air.

Comparison of the current densities from cyclic voltammetry at −0.6 V vs. Pt/Air in 0.1% NO in Ar and in air shows that all the electrodes have increasing selectivity towards NO with decreasing temperature. Furthermore, the results indicate that the $(La_{0.5}Sr_{0.5})_{0.99}MnO_3$ (LSM50)/$Ce_{0.8}Pr_{0.2}O_2$ electrode has the highest selectivity in the temperature range of 300–400 °C.

Acknowledgement This work was supported financially by The Programme Commission on Sustainable Energy and Environment, The Danish Council for Strategic Research, via the Strategic Electrochemistry Research Center (www.serc.dk), contract no. 2104-06-0011.

References

1. Pancharatnam S, Huggins R, Mason D (1975) Catalytic decomposition of nitric oxide on zirconia by electrolytic removal of oxygen. J Electrochem Soc 122:869–875
2. Gür T, Huggins R (1979) Decomposition of nitric oxide on zirconia in a solid-state electrochemical cell. J Electrochem Soc 126:1067–1074
3. Reinhardt G, Wiemhöfer HD, Göpel W (1995) Electrode reactions of $La_{0.8}Sr_{0.2}MnO_{3-\delta}$-electrodes on stabilized zirconia with oxygen and the nitrogen oxides NO and NO_2. Ionics 1:32–39
4. Hibino T (1994) Electrochemical removal of both NO and CH_4 under lean-burn conditions. J Appl Electrochem 25:203–207
5. Wachsman E, Jayaweera P, Krishnan G, Sanjurjo A (2000) Electrocatalytic reduction of NO_x on $La_{1-x}A_xB_{1-y}B'_yO_{3-\delta}$: evidence of electrically enhanced activity. Solid State Ionics 136–137:775–782
6. Teraoka Y, Harada T, Kagawa S (1998) Reaction mechanism of direct decomposition of nitric oxide over Co- and Mn-based perovskite-type oxides. J Chem Soc, Faraday Trans 94:1887–1891
7. Ishihara T, Ando M, Sada K, Takishii K, Yamada K, Nishigushi H, Takita Y (2003) Direct decomposition of NO into N_2 and O_2 over La(Ba)Mn(In)O_3 perovskite oxide. J Catal 220:104–114
8. Tofan C, Klvana D, Kirchnerova J (2002) Direct decomposition of nitric oxide over perovskite-type catalysts Part I. Activity when no oxygen is added to the feed. J Appl Catal A 223:275–286
9. Nauer M, Ftikos C, Steele B (1994) An evaluation of Ce–Pr oxides and Ce–Pr–Nb oxides mixed conductors for cathodes of solid oxide fuel cells: structure, thermal expansion and electrical conductivity. J Eur Ceram Soc 14:493–499
10. Stefanik T, Tuller H (2000) Ceria-based gas sensors. J Eur Ceram Soc 21:1967–1970
11. Krishna K, Bueno-López A, Makkee M, Moulijn J (2007) Potential rare-earth modified CeO_2 catalysts for soot oxidation. Top Catal 42–43:221–228
12. Mizusaki J, Yonemura Y, Kamata H, Ohyama K, Mori N, Takai H, Dokiya M (2000) Electronic conductivity, Seebeck coefficient, defect and electronic structure of nonstoichiometric $La_{1-x}Sr_xMnO_3$. Solid State Ionics 132:167–180
13. Fagg D, Marozau I, Shaula A, Kharton V, Frade J (2006) Oxygen permeability, thermal expansion and mixed conductivity of $Gd_xCe_{0.8-x}Pr_{0.2}O_{2-\delta}$. J Solid State Chem 179:3347–3356
14. Chick L, Pederson LR, Maupin GD, Bates JL, Thomas LE, Exarhos GJ (1990) Glycine-nitrate combustion synthesis of oxide ceramic powders. Mater Lett 10:6–12
15. Winkler J, Hendriksen P, Bonanos N, Mogensen M (1998) Geometric requirements of solid electrolyte cells with a reference electrode. J Electrochem Soc 145:1184–1192
16. Werchmeister R, Hansen K, Mogensen M (2010) Characterisation of $La_{1-x}Sr_xMnO_3$ and doped ceria composite electrodes in NO_x containing atmosphere with impedance spectroscopy. J Electrochem Soc 157:P35–P45
17. Clausen C, Bagger C, Bilde-Sørensen J, Horsewell A (1994) Microstructural and microchemical characterization of the interface between $La_{0.85}Sr_{0.15}MnO_3$ and Y_2O_3-stabilized ZrO_2. Solid State Ionics 70(71):59–64
18. Boukamp B (1986) A nonlinear least squares fit procedure for analysis of immitance data of electrochemical systems. Solid State Ionics 20:31–44
19. Barsoukov E, MacDonald J (2005) Impedance spectroscopy—theory, experimental and applications, 2nd edn. Wiley Interscience, New York
20. Jacobsen T, Zachau-Christensen B, Bay L, Skaarup S (1996) In: Poulsen FW, Bonanas N, Linderoth S, Mogensen M, Zachau-Christensen B (eds) SOFC Cathode Mechanisms, Proc 17th Risø int symp on materials science. Risø National Laboratory, Roskilde, Denmark, pp 29–40
21. Primdahl S, Mogensen M (1998) Gas conversion impedance: a test geometry effect in characterization of solid oxide fuel cell anodes. J Electrochem Soc 145:2431–2438
22. Hansen KK, Skou E, Christensen H, Turek T (2001) Perovskites as catalysts for the selective catalytic reduction of nitric oxide with propene: relationship between solid state properties and catalytic activity. J Catal 199:132–140